Optimisation of Novel Elliptically-Based Web Opening Shapes of Perforated Steel Beams

Konstantinos Daniel Tsavdaridis[1], Cedric D'Mello[2]

[1] *School of Engineering and Mathematical Sciences, City University London, EC1V 0HB, UK, Office: C354, E-mail: konstantinos.tsavdaridis.1@city.ac.uk*

[2] *School of Engineering and Mathematical Sciences, City University London, EC1V 0HB, UK, Office: C173, E-mail: C.A.Dmello-1@city.ac.uk*

A B S T R A C T

A new study was carried out and presented herein, on the optimisation of novel elliptically-based web opening shapes which enhance the structural behaviour of the perforated beams as well as lead to economic design in terms of both manufacture and usage.

The finite element (FE) model used in the study was validated against experimental work conducted by the authors and the results of the comprehensive study are presented in this research paper. For ease of comparison, the yield patterns and deflected shapes of the perforated beams are presented at three 'characteristic' load level points. Finally, shear-moment interaction FEM curves are presented for six novel web opening shapes to allow for easy use of the empirical design formulas that have previously been proposed by the authors in a complementary research paper.

An overall study of many standard and non-standard web opening shapes, it was shown that perforated beams with vertical and inclined classic elliptical web openings (3:4 width to depth ratio) behave more effectively compared to perforated beams with conventional circular and hexagonal web openings, mainly in terms of stress distribution and local deflection. Therefore, perforated steel beams with large novel elliptically-based web openings with short critical opening length at the top and bottom tee-section as well as straight-line edges are presented for first time and examined in the current research programme.

1. Introduction

1.1 Advantages

Since the 1940s many attempts have been made by structural engineers to find new ways to reduce the cost of steel structures. Due to limitations on maximum allowable deflections, the high strength properties of structural steel cannot always be utilised to the best advantage. As a result, several new methods have been aimed at increasing the stiffness of steel members without any increase in the weight of steel required. Hence, castellated and cellular beams have been used extensively in recent times.

It is recognised that the ease of integration of services, such as hydraulic and ventilation pipes as well as electric cables, within the structural depth of the beams provides a major benefit in the construction. The effect is that the overall building height is reduced, by the decrease in the floor to ceiling height for every storey level, compared to the conventional plain webbed beam usage where the services are supported beneath the beam. Typical savings in such terms could be up to half a metre per storey level.

The outcome of this is a more sustainable and economic construction method. Moreover, there have been significant improvements in the structural design of commercial multi-storey buildings in recent years, based on the development of long span composite systems. Long span beams have the advantage of flexibility of internal planning by limiting the number of columns resulting in savings in the number of foundations and in speed and cost of erection. Long span beams are more competitive in the industry, mainly when they are manufactured for car parking structures, curved roof beams or stadium cantilever roof tapered beams.

The manufacturing method [1, 2] of the aforementioned perforated beams is a very important factor as it affects the cost and the structural behaviour of the final product. Many advantages are gained by using the profile cutting procedure to manufacture a perforated steel beam, but this process needs to be optimised to keep costs down. The well used profile cutting procedure for the fabrication of perforated beams is considered in this paper and the novel web opening shapes are specifically designed to improve it in terms of cost and time [3].

2. Introduction to present study

2.1 Aims

The aim of this research work is to investigate the behaviour of perforated steel beams with different novel web opening shapes and in particular, to optimise these shapes for beams that are subject to high shear forces. These novel web opening shapes are based on an elliptical configuration and are in line with the profile cutting manufacturing procedure of steel perforated beams. The shape optimisation was investigated through comprehensive parametric studies in order to achieve a light structural member with high load carrying capacity.

2.2 Novel web opening shapes

Apart from the structural engineering advantages gained incorporating elliptical web opening shapes into perforated steel beams, the novel web opening configuration should also be ideal for simple and economic fabrication. Perforated beams with circular web openings are widely used in the steel construction industry, as they provide smooth stress distribution in the vicinity of the web openings and a large web opening area. However, perforated beams with circular web openings produce a significant amount of scrap steel during their fabrication, especially when the profile cutting procedure is used. The profile cutting procedure becomes also expensive when a full two-way oxy-cut is utilised. Moreover, the welding procedure is sometimes difficult, as the automated welding machines are not able to identify the first welding start-point between the top and bottom tee-sections on the uniform smooth circular edge.

The novel elliptically-based web opening shapes introduced have a narrow opening length at the top and bottom tee-sections (**Fig. 1**). These web opening shapes consist of a combination of semi-circles with straight lines. In elliptical shapes the width is independent of the depth and many deep web openings can be fitted adjacent to each other along the length of a beam, in comparison with the perforated beams with circular web openings. Therefore, the stiffness of the web-posts is not reduced whilst the weight of the beam is effectively reduced [4], as it is usually required for long span applications in avoiding large deflections due to self-weight.

To define the various web opening configurations with different web opening areas, two main parameters are varied: the angle (θ) of the straight lines and the radius (R) of the semi-circles at the top and bottom tee-sections. Four θ angles (10^o, 20^o, 30^o and 40^o) as well as four R radii ($0.15d_o$, $0.2d_o$, $0.25d_o$ and $0.3d_o$) and their combinations were modelled for now. The elliptical form of these web openings was investigated in both the vertical and inclined configurations.

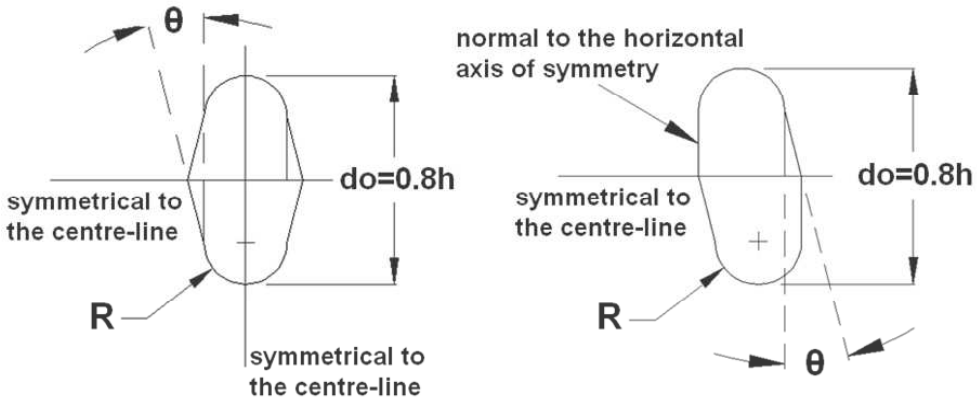

Fig. 1: Geometric parameters (Angle, θ and radius, R)

2.3 Specimens for optimisation study

High shear-moment (V/M) interaction was applied to the centre-line of the isolated web-openings to study the Vierendeel mechanism behaviour.

Sixteen different web openings were modelled covering the vertical elliptical configuration. The same concept was followed for the development of the inclined elliptical web openings, where the top and bottom tee-sections (i.e. semi-circles with radius, R) are moved in opposite directions and form an inclined elliptical shape. The distance of this movement depends on the angle, θ. The concept for the inclined elliptical web opening shapes is based on previous studies [4, 5, 6, 7], which showed that inclined elliptical web openings can behave better than vertical ones in certain cases. The same orientation of the two symmetrical to the mid-span web openings was chosen (i.e. they are not mirrored) so as to be able to study both deflected shapes and stresses in the vicinity of the web openings when the beam is loaded. This configuration does not represent the worst case scenario; however the difference can be ignored. Additionally, a perforated beam with circular web openings and diameter, d_o, equal to $0.8h$, was modelled for direct comparison. In total thirty-three FE models were analysed to optimise the shape of the novel elliptical web openings. It is anticipated that some perforated beams will present significant high stress concentration at specific points due to the particular combination of R and θ, and they should be carefully considered for further study.

3. Validation of the FE model for Vierendeel failure of perforated beams

3.1 General failure modes of perforated steel beams

To date, experimental and finite element studies on perforated beams have reported six main different modes of failure [8, 9, 10, 11]. These modes are closely associated with beam geometry, shape parameters, web slenderness, type of loading, and provision of lateral supports. Under given applied transverse or coupling forces, failure is likely to occur by one of the following modes:

- Vierendeel or Shear Mechanism
- Flexural Mechanism
- Lateral Torsional Buckling (LTB)
- Rupture of Welded Joints
- Web-post Buckling in Shear

- Compression Buckling

The local carrying capacity of a perforated beam may be limited by the local bending and shear strength of the web-posts, top and bottom tee-sections. These likely weak areas are indicated in **Fig. 2** which also illustrates all key parameters; some of them are presented in this research.

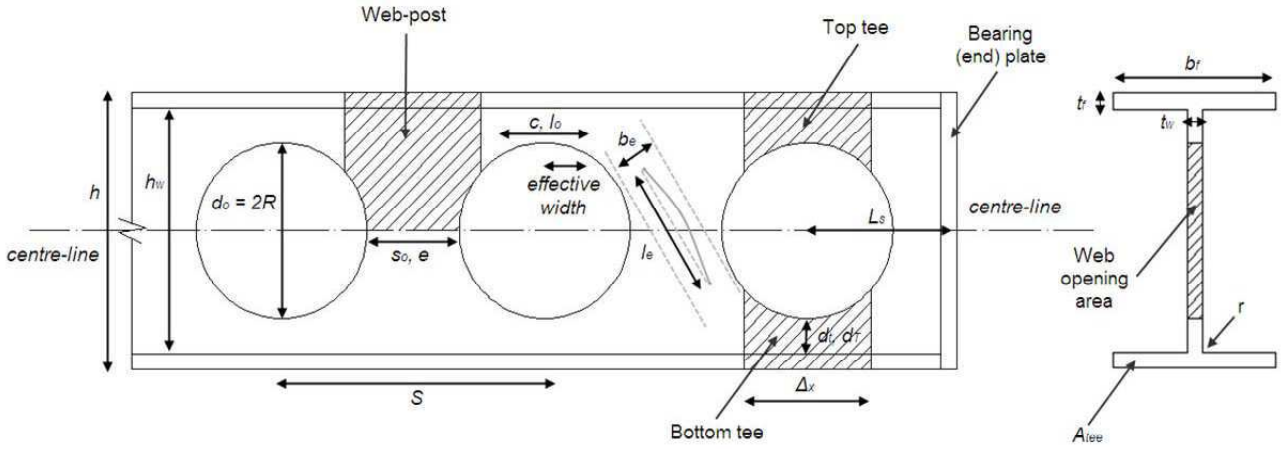

Fig. 2: Important areas and geometrical key parameters

3.2 Vierendeel mechanism

This paper focuses on the structural behaviour of perforated beams that tend to fail with the formation of a Vierendeel mechanism. Vierendeel bending is caused by the need to transfer the shear force across the web openings to be consistent with the rate of change of the bending moment along the beam, and it is the most dominant failure mode of perforated beams with isolated large web openings. It is also a common failure mode when perforated steel beams with widely spaced web openings support concrete slabs from below in traditional composite flooring systems in steel structures. In the absence of local or overall instability, perforated beams with web openings have two basic modes of collapse which depend upon the geometry and the position of the web opening [12]. They are:

- Plastic tension and compression stress blocks in the top and bottom tee-sections in regions of high overall buckling (**Fig. 3(a)**).
- Parallelogram or Vierendeel action due to the formation of plastic hinges at the four corners or at specific angles around the web opening, in regions of high shear (**Fig. 3(b)**).

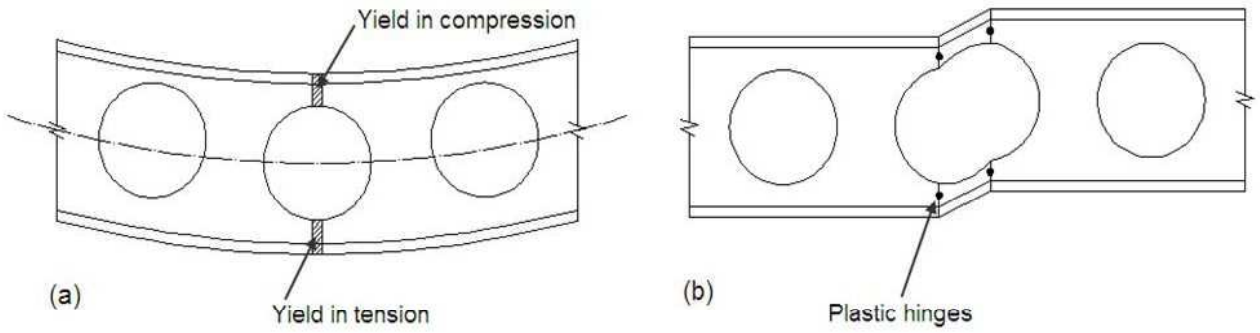

Fig. 3: (a) Yielding due to high bending and (b) Yielding due to high shear (adopted by [12])

3.3 Behaviour of perforated beams

In the case of using the profile cutting method to manufacture perforated beams, the two half tee-sections are shifted and then welded together to produce a beam of a greater depth with hexagonal or circular openings in the web. The final beam has a larger section modulus and greater bending rigidity than the original (plain webbed) section as well as the final product is a lighter beam. However, the presence of the web openings changes the structural behaviour of the beam from that of the plain webbed beams. Various experimental tests on castellated and cellular beams have shown that beam slenderness, web opening configuration and the loading type are the main parameters, which dictate the strength and the failure modes of such beams.

Structurally, web openings cause a significant reduction to the shear resistance of beams, due to the loss of a major proportion of the web, but they cause a smaller reduction in the bending resistance of beams. Therefore, shear transfer across sections with large web openings is an important design requirement.

Vierendeel bending results in the formation of four plastic hinges above and below the web opening. The overall Vierendeel bending resistance depends on the local bending resistances of the web-flange sections. As the global shear forces cause both shear failure and Vierendeel mechanism in perforated sections, the effect of local Vierendeel moments acting onto the "corners" of the tee-sections above and below the web openings may be incorporated through a reduction to the global shear capacities of the perforated sections. The shear capacity which governs the global shear capacity of a perforated section under shear failure and Vierendeel mechanism in the absence of global moment called 'coupled' shear capacity [13].

It is known that the shear and flexural failures of typical perforated sections are controlled mainly by the size (i.e. depth, d_o) of the web openings, whilst the Vierendeel mechanism is primarily controlled by the critical length, c, of the tee-sections. However, from another study [5] it was found that perforated beams with non-standard shapes of web openings could behave differently and that the shear to moment interaction and the local failure mode are directly dependent upon the actual web opening configuration.

A detailed sensitivity study of the geometric parameters, which construct these novel web opening shapes was carried out and the results are analysed to determine the most effective web opening configurations. The beams examined were designed so that they experience high shear forces at the centre-line of the web openings and Vierendeel mechanism is fully formed.

In the case of perforated beams with web openings placed next to each other (i.e. closely spaced), the combination of forces acting on the edges of the web openings is quite complex and a complementary study on selected novel elliptically-based web openings was published recently by the authors [4].

3.4 Methodology

In order to provide information on the structural performance of perforated beams with novel web opening configurations, it was important to undertake a comparative study between the standard (i.e. beams with circular and hexagonal web openings) and the new structural forms. Common mid-range universal beam (UB) sections utilised for roof and floor applications were validated for the investigation.

Hot rolled symmetric I-sections of class 1 or 2 (plastic or compact) with isolated web cut-outs were examined, in which the two openings are located symmetrically at both ends of the beams. All web openings are concentric to the mid-depth of the sections with a depth of d_o, equal to $0.8h$, where h is the section height. The comparison was made at three 'characteristic' load levels, at which deflections and stresses were acquired. The structural adequacy of the steel perforated beams was in accordance of the

section capacities under co-existing global shear forces and moment. Hence, both the bending moment, $M_{o,Sd}$, and the shear force, $V_{o,Sd}$, due to global actions are evaluated at the vertical centre-line of the web openings.

It is worth noting that although most of the advantages of using the particular perforated beams with novel web opening shapes are gained when the profile cutting procedure is used, isolated cut-outs were modelled for this study in order to avoid recording failure modes other than that of the Vierendeel mechanism (eg. failure under complex actions from adjacent web openings), as well as to limit the number of geometric parameters (eg. web opening spacing, final increased height of the welded section, etc.). The FE model was correlated against the experimental work conducted by the authors [14]. The elaborate FE model was then used for a parametric study optimising the particular novel web opening shapes and further used to develop simple *V/M* non-dimensionalised interaction curves which can be readily used in engineering practice, following a simple design method proposed earlier [5].

3.5 Experimental programme

3.5.1 Test specimen

Steel section, UB305x165x40 (S355) was tested in a configuration that ensured that the web openings were subjected to high shear forces with the formation of four Vierendeel plastic hinges being expected [14]. The web opening diameter, d_o, of the circular web openings, was equal to *0.76h*, the maximum diameter found in practice. The end distance between the web openings and the centre-line of the support was equal to $1.3d_o$, in line with design rules. The beam was symmetrical about mid-span.

3.5.2 Coupon tests

Tensile coupon tests were carried out according to the specifications and guidelines [15]. Coupon samples were taken from four un-yielded locations of the tested steel perforated beam. The samples are taken from the overhang web and the compression flange at mid-span. **Table 1** summarizes the physical properties obtained from tensile tests.

Specimen Represented	Coupon No.	Yield Strength, f_y (MPa)	Tensile Strength, $f_{ult.}$ (MPa)	Average Yield Strength, f_y (MPa)	Average Tensile Strength, $f_{ult.}$ (MPa)
Web	**1**	297	415	299	413.5
	2	301	412		
Flange & Bearing Plate	**1**	339	450	337.5	448
	2	336	446		

Table 1: Measured material physical properties

3.5.3 Test rig setup

The test setup was a single-span beam under bending with both ends simply supported resulting in a statically determinate system. The load was applied through two hydraulic jacks on the load spreader plate with roller supports at the ends. The applied loading was measured through load cells connected to the jacks and displacements were recorded at key positions with the use of three dial gauges.

3.5.4 Load-deflection relationships

Linear behaviour was observed up to 176.2kN, which is the 64.2% of the "ultimate load carrying capacity" of the beam. At 256kN local buckling at compression points at the edge of the web opening had taken place, together with yielding of the compression flange above the web openings. This was due to the

high Vierendeel bending forces in the section. The overall flexural failure mode and the locally distorted web and flanges of the steel section, as well as the elongation of the circular web opening shape are illustrated in **Fig. 4.**

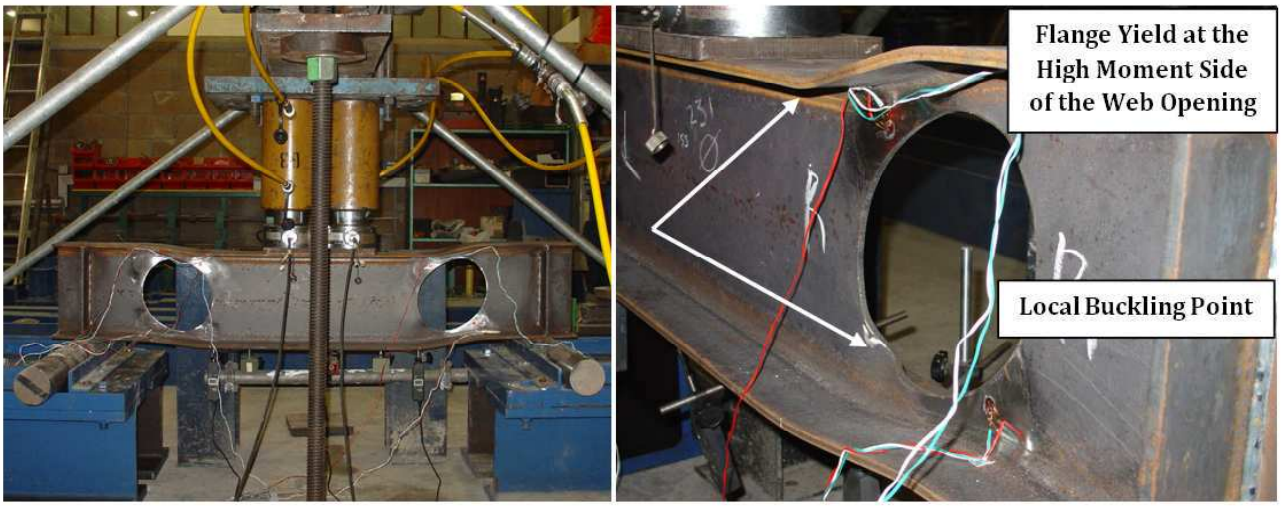

Fig. 4: Flexural failure with local highly distorted web - flanges

3.6 Validation of the FE model against experimental work

3.6.1 Description of the FE model

In order to simulate the structural behaviour of the experimental setup, a FE model was developed in a commercial FE analysis software package, ANSYS v10.0. The FE model of the steel beam used to perform the parametric study of the web opening shape optimisation, was first validated by conducting a non-linear elasto-plastic analysis and comparing it with the results of the experimental test above. The key points of the non-linear analyses carried out are summarised below:

- ANSYS SHELL181 (4-node) elements with a quadratic deformation approach were used.
- The influence of meshing and its refinement was addressed through convergence study.
- An iterative Newton-Raphson method with a large deformation approach was used as the solution technique.
- Modelling the elasto-plastic (Bilinear Kinematic Hardening) material properties two methods were approached:
    - The averaged yield and ultimate tensile material properties from **Table 1** were used to model the beam. Averaged physical properties (actual curve: f_y=*318.25MPa* and $f_{ult.}$=*430.75MPa*) used for web, flanges and bearing plates are shown in **Fig. 5.** The Young's Modulus, *E*, was taken as 200GPa and the Tangent Modulus, E_T, as 2000MPa.
    - For further comparison of the FE model and to generalise the results, nominal values were used for the material properties. Therefore, it was assumed that the beam is of grade S355, uniform across the section and with the following material properties: *E=200GPa*, *v=0.3*, f_y=*355MPa* and $f_{ult.}$=*530MPa* and E_T=*2000MPa* (idealised curve).

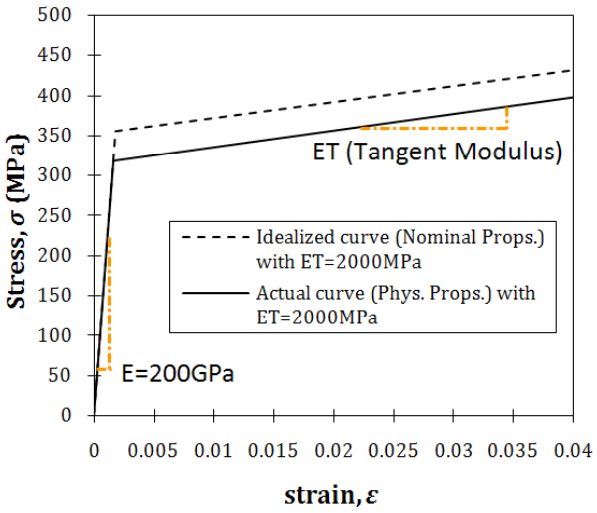

Fig. 5: Idealised bi-linear stress-strain curve

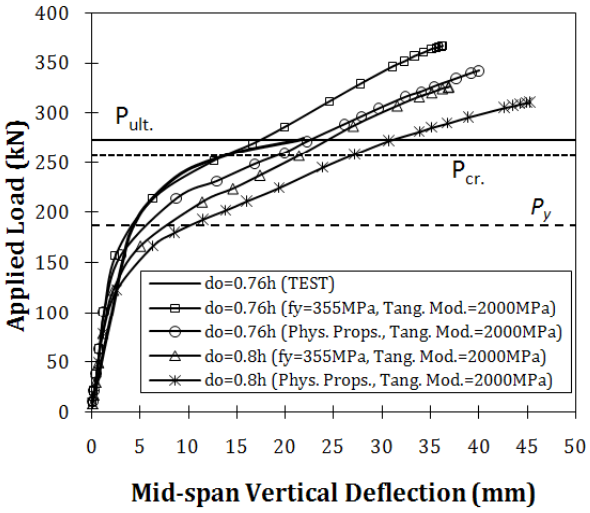

Fig. 6: Load-deflection curves

It is interesting to note that the steel beams provided by the manufacturers were of steel grade S355 (f_y=*355MPa* and $f_{ult.}$=*530MPa*) but the tensile coupon tests showed that the yield and tensile strengths of the web, flanges and welded bearing plates vary (**Table 1**). Therefore, the FE model and the non-linear analysis techniques should be verified to ensure that the model is capable of predicting the required mode of behaviour within the parametric study. Hence, it was decided to average the yield and tensile material properties and compare that to a FE model using the nominal material properties of S355 steel grade. The general idea in this research project is to provide a simple generic FE model which can give reliable results when researchers use the nominal material properties in conducting sensitivity studies of the geometric parameters of the novel web opening shapes.

Special attention was given to the meshing of the perforated beams and especially in the vicinity of the novel web openings as their shape is based on the elliptical form and it is a mix of both straight lines and curves. Therefore, a mesh convergence study was required for all FE beam models with manually meshed areas (mapped meshing) to keep the shape and the size of the elements consistent.

3.6.2 Results

The load-deflection curves obtained from the FE models with both web openings sizes and d_o equal to *0.76h* and *0.8h*, together with the tested specimen with d_o equal to *0.76h* are plotted in **Fig. 6** for direct comparison. It is seen that the FE models showed higher stiffness in the plastic region. This is due to the fact that a bi-linear material property with the yield and the ultimate tensile material strengths was used to model the elasto-plastic material behaviour of the steel. Hence, the FE calculations stopped either when the ultimate tensile stress values were reached (i.e. $f_{ult.}$=*530MPa*), the node's displacement exceeded the default (by ANSYS) values, or the displacement started to increase very rapidly without sufficient load increase. Consequently, increased strain hardening was observed in the plastic region before the FE models finally stopped/converged. At the point of the so called "ultimate load carrying capacity" of the test (274.4kN), the dial gauge located at the mid-span had reached its travel distance length and suddenly de-attached. In reality, the beam would have kept on deflecting in the vertical plane, even though it was considered that it has failed (i.e. reached its ultimate capacity) as high deformations at local buckling points were previously observed. It is worth to note that the FE model with the nominal material properties of steel grade S355 models accurately the test (**Fig. 6**).

It is also interesting to examine the local displacement vectors and their magnitudes (**Fig. 7**), as well as the stress distribution (**Fig. 8**) in the vicinity of the web openings at failure loading point, as taken from the FE analysis, to thoroughly understand the stress distribution and the formation of the plastic hinges.

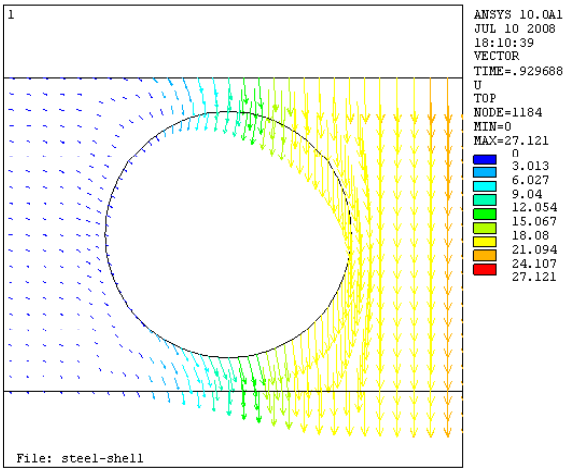

Fig. 7: Displacement vectors

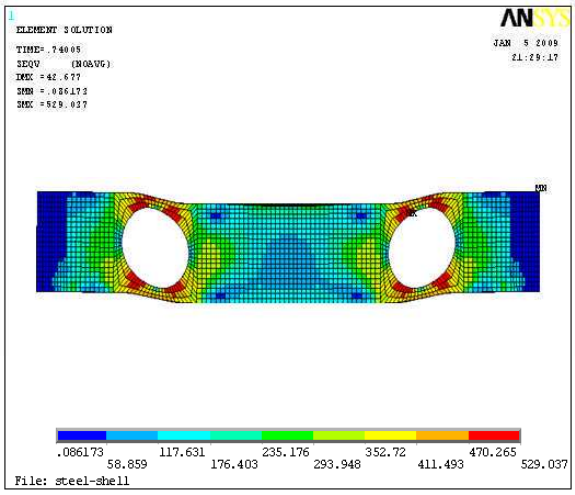

Fig. 8: Von-Mises stresses at failure load

4. Parametric FE study to optimise the novel web opening shape

4.1 Method of study

It is difficult to find the best combination of the geometric parameters of the novel web opening shapes and it is complicated to achieve this due to mathematical complexity in dealing with many unknowns and formulas. Finite element analysis enables us to avoid such problems. The validation of the FE model against the experimental work and the agreement of the results provide reliability to the novel beam models.

In order to be able to understand the results of the optimisation study, it was decided to examine stresses and deflections at three different 'characteristic' load levels. This was achieved by using three benchmark load levels as obtained from the experimental testing of the typical perforated beam with circular web openings of diameter, d_o, equal to *0.76h.* The 'characteristic' load levels are presented in **Table 2** and depicted in **Fig. 6** (P_y*=176.2kN*, $P_{cr.}$*=256kN* and $P_{ult.}$*=274.4kN*). The load P_y indicates the experimental value when first yielding at the edges of the circular web openings occurs. Furthermore, the yield load, P_y, indicates that both the web and the flange sections will yield completely. The buckling load, $P_{cr.}$, of the web and the flanges is determined from the records of the deflection (dial) gauges underneath the tension flange located at the high moment side of each web opening. The yield load P_y is smaller than $P_{cr.}$ and $P_{ult.}$, because the edges of the circular web openings carry additional moments by Vierendeel action and longitudinal shear forces (full plastic hinge formation), in addition to the normal bending moment and vertical shear force. Therefore, it appears that this local yielding of the edges is directly related to the ultimate strength of the beam.

Conceptually, the differences between the perforated beams with circular web openings of both diameters and the perforated beams with the novel web openings shapes can be rationally evaluated. The Von-Mises stresses, σ, and the maximum vertical deflections, δ, at these aforementioned load levels are recorded in **Table 2**, **Table 3** and **Table 5** and presented in **Fig. 9** to **14.**

4.2 Results for vertical elliptical novel web openings

Up to the point of the 'characteristic' yield load, the stiffness of all perforated beams is similar. However, significant deviation of the results was observed in the plastic region, due to the large Tangent Modulus in combination with the large deformation approach in the FE solution technique activating the full non-linear geometric behaviour. This allows for load redistribution in the web across the web openings after initial yielding.

From **Table 3** it can be seen that perforated beams with vertical elliptical web openings of different combinations of θ and R have similar deflections at low load levels. It is noted that some of these beams experience similar stresses too, whilst the web opening areas are different.

Fig. 9 to **11** present the FE results of Von-Mises nodal stresses and maximum vertical deflections. The results are given in sequence, starting with the web opening shape which provides the smallest web opening area (i.e. specimen No.1). The specimen numbers and the web opening areas are summarised in **Table 4**, together with the ratio of percentage compared to the circular web opening with diameter, d_o, equal to $0.8h$.

	at P_y=176kN		at $P_{cr.}$=256kN		at $P_{ult.}$=274.4kN		at FEA Solution Divergence		
	Max. δ (mm)	**Von-Mises stress, σ (MPa)**	**Max. δ (mm)**	**Von-Mises stress, σ (MPa)**	**Max. δ (mm)**	**Von-Mises stress, σ (MPa)**	**Load, P (kN)**	**Max. δ (mm)**	**Von-Mises stress, σ (MPa)**
TEST MODEL CIRCULAR $d_o=0.76h$	3.8	-----	13.6	-----	21.8	-----	-----	-----	-----
FEM CIRCULAR $d_o=0.76h$	3.6	372.8	13.6	453.7	21.8	510.3	293	32.4	529
FEM CIRCULAR $d_o=0.8h$	6	398.6	21	522.5	24.7	526.6	339.4	41.1	529.7

Table 2: Characteristic load levels for comparison and benchmark FE models

		at P_y=176kN		at $P_{cr.}$=256kN		at $P_{ult.}$=274.4kN		at FEA Solution Divergence		
	R/d_o	Max. δ (mm)	Von-Mises stress, σ (MPa)	Max. δ (mm)	Von-Mises stress, σ (MPa)	Max. δ (mm)	Von-Mises stress, σ (MPa)	Load, P (kN)	Max. δ (mm)	Von-Mises stress, σ (MPa)
Angle $\theta = 10^o$	0.15	1.4	369.1	3.9	408	4.7	429.9	392	20.1	529.8
	0.2	1.9	371.7	3.3	422.3	6.8	446.7	380	23.4	529.7
	0.25	1.9	366.5	4.5	402.7	5.8	418.5	386	21.7	529.1
	0.3	2.8	378	10	466.4	13.7	506.1	382	34	529.8
Angle $\theta = 20^o$	0.15	1.4	368.9	3.9	408	4.7	429.9	394	20.1	529.9
	0.2	1.9	371.2	3.3	420.7	6.8	444.6	382	24.2	529.7
	0.25	2.2	374.1	6.2	440.7	10	477.1	389	30.3	529.8
	0.3	2.8	377.6	10	465.4	13.7	504.9	384	34.7	530
Angle $\theta = 30^o$	0.15	1.5	379.6	4.5	440.8	5.8	466.4	377	17.7	530
	0.2	1.5	370.6	3.3	419.2	6.8	440.9	384	24.4	529.8
	0.25	2.2	374.6	6.2	438	10	476.3	384	29.3	529.8
	0.3	2.8	377.3	10	463.5	13.7	502.3	375	32.7	529.8
Angle $\theta = 40^o$	0.15	2.2	369.3	4.2	410	5.2	430.5	384	20.1	529.8
	0.2	1.9	371.9	3.3	422.8	6.8	447.1	377	23.7	529.6
	0.25	2.2	373.3	6.2	435.9	10	470.1	379	28.5	529.6
	0.3	2.8	376.9	10	461.3	13.7	500.2	382	34.4	529.9

Table 3: Initial evaluations for perforated beams with circular web openings

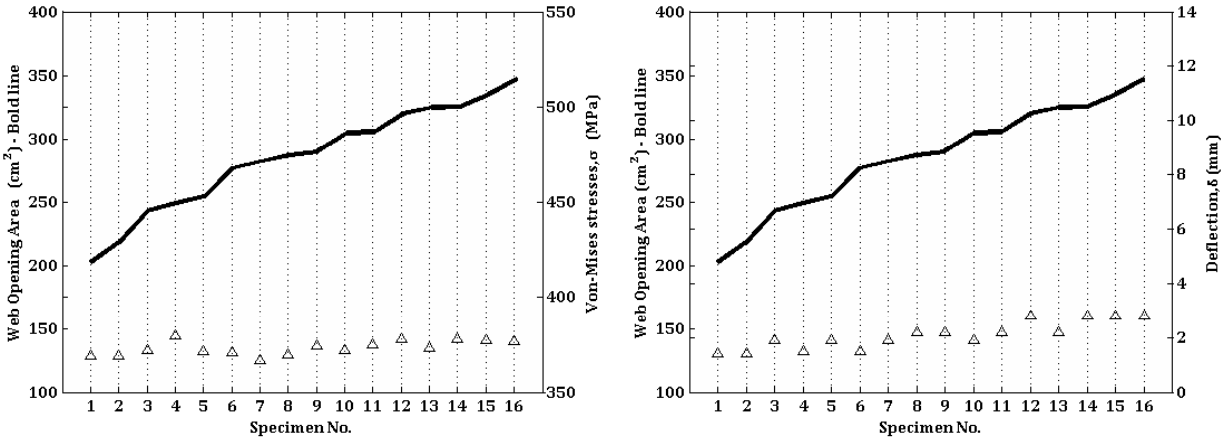

Fig. 9: Von-Mises nodal stresses (left) and maximum vertical deflections (right) at P_y

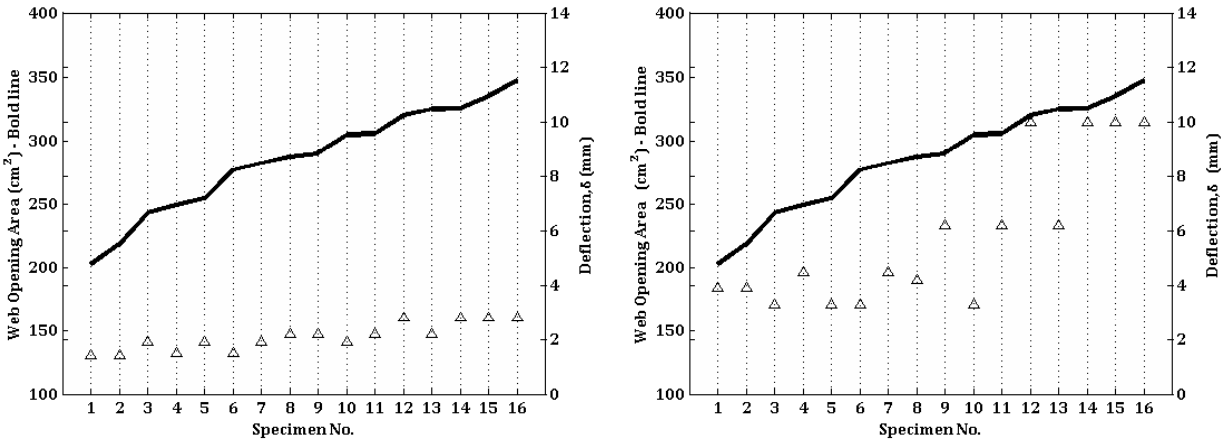

Fig. 10: Von-Mises nodal stresses (left) and maximum vertical deflections (right) at $P_{cr.}$

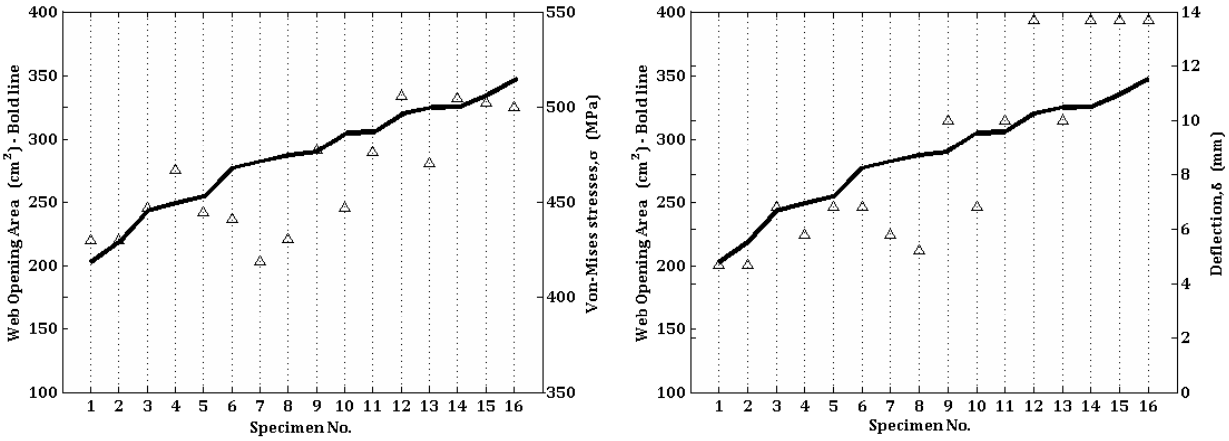

Fig. 11: Von-Mises nodal stresses (left) and maximum vertical deflections (right) at $P_{ult.}$

Specimen No.	Novel elliptical web openings (d_o=0.8h)		Specimen No.	Novel elliptical web openings (d_o=0.8h)		Ratio of Novel/Circular web openings, d_o=0.8h	
						d_o=0.76h	d_o=0.8h
	Vertical	Area (cm^2)		Inclined	Area (cm^2)	A=419.1cm^2	A=460cm^2
1	*θ10&R0.15*	202.6	1	*θ10&R0.15*	184	0.44	0.40
2	*θ20&R0.15*	217.9	2	*θ20&R0.15*	191.6	0.47	0.42
3	*θ10&R0.2*	242.8	3	*θ30&R0.15*	207	0.53	0.45
4	*θ30&R0.15*	248.7	4	*θ40&R0.15*	225.9	0.54	0.49
5	*θ20&R0.2*	254	5	*θ10&R0.2*	229.1	0.55	0.50
6	*θ30&R0.2*	276.6	6	*θ20&R0.2*	234.7	0.60	0.51
7	*θ10&R0.25*	282	7	*θ30&R0.2*	246	0.61	0.53
8	*θ40&R0.15*	286.5	8	*θ40&R0.2*	259.9	0.62	0.57
9	*θ20&R0.25*	289.8	9	*θ10&R0.25*	272.5	0.63	0.59
10	*θ40&R0.2*	304.4	10	*θ20&R0.25*	276.4	0.66	0.60
11	*θ30&R0.25*	305.5	11	*θ30&R0.25*	284.2	0.66	0.62
12	*θ10&R0.3*	320.1	12	*θ40&R0.25*	293.9	0.70	0.64
13	*θ40&R0.25*	324.8	13	*θ10&R0.3*	314	0.71	0.68
14	*θ20&R0.3*	325.1	14	*θ20&R0.3*	316.5	0.71	0.69
15	*θ30&R0.3*	335.2	15	*θ30&R0.3*	321.6	0.73	0.70
16	*θ40&R0.3*	347.5	16	*θ40&R0.3*	327.7	0.76	0.71

Table 4: Numbering the corresponding novel web opening shapes and their web opening areas

It was observed that the increase of load carrying capacity depends more on the radius of the semi-circles, R, rather than on the angle of the straight-lines, θ. Maximum vertical deflections of perforated beams with novel web openings are significantly smaller than the ones obtained from perforated beams with typical circular web openings of both diameter sizes. In contrast, perforated beams with circular web openings provide a smooth transition of the stresses at the edge of the web openings, and hence in some cases, the novel perforated beams behave worse in terms of stress concentration. The variation of the stresses is based mainly on the specific combination of R and θ and it should be carefully considered.

As the load is increased, the deflections are more sensitive to the change of R. It was also found that the bigger the radius, R, the higher the deflections are. The main reason is that the critical opening length, c, (**Fig. 2**) is increased and hence the Vierendeel action is severe. Also, by increasing the radius, R, the web opening area is significantly increased, whilst the stiffness of the perforated section is decreased.

In particular it is worth noting that the specimens No.7 and No.8 present remarkably small deflections and stresses, whilst on the other hand the specimens No.4 and No.12 present significantly increased stresses. The reason for this different behaviour is the high stress concentration at the sharp corners points on the web opening edge, created by the combination of the specific θ and R.

4.3 Results for inclined elliptical novel web openings

Similarly, stresses and deflections at the three different 'characteristic' load levels are presented in **Table 1. Table 5** shows that there are various perforated sections with different θ but same R geometric parameters, which deflect similarly at certain 'characteristic' load levels as well as they are governed by similar stress levels.

Fig. 12 to **14** demonstrate the FE results of Von-Mises nodal stresses and maximum vertical deflections. The numbers of the specimens and their opening area are summarised in **Table 4.**

	R/d_o	at P_y=176kN		at $P_{cr.}$=256kN		at $P_{ult.}$=274.4kN		FEA Solution Divergence		
		Max. δ (mm)	Von-Mises stress, σ (MPa)	Max. δ (mm)	Von-Mises stress, σ (MPa)	Max. δ (mm)	Von-Mises stress, σ (MPa)	Load, P (kN)	Max. δ (mm)	Von-Mises stress, σ (MPa)
Angle $\theta = 10^o$	**0.15**	1.6	369.2	4	407.9	4.8	429.8	391	19.9	529.9
	0.2	2	372.4	5.5	423.9	6.8	448.6	377	23.4	529.6
	0.25	2.5	374.6	7.3	442.5	10	479.6	387	29.8	529.8
	0.3	3	378.3	10.3	467.3	13.8	507.1	384	34.5	529.8
Angle $\theta = 20^o$	**0.15**	1.6	369.5	4	408.7	4.8	437.9	383	19.1	529.8
	0.2	2	372.5	5.5	425.5	6.8	448.3	383	24.3	530
	0.25	2.5	374.4	7.3	442.1	10	479.5	383	29.1	529.8
	0.3	3	378.2	10.3	467	13.8	506.5	384	34.7	530
Angle $\theta = 30^o$	**0.15**	1.6	369.7	4	410.7	4.8	430.1	391	20.3	529.8
	0.2	2	372.2	5.5	423.7	6.8	446.8	384	24.5	530
	0.25	2.5	375.1	7.3	442.7	10	478.7	391	30.4	529.9
	0.3	3	377.9	10.3	465.6	13.8	506	387	35	529.9
Angle $\theta = 40^o$	**0.15**	1.6	369.4	4	407.9	4.8	428.1	391	20.6	529.8
	0.2	2	371.2	5.5	425.3	6.8	447.6	385	24.9	529.8
	0.25	2.5	374.6	7.3	442.2	10	479.2	389	30.4	529.9
	0.3	3	378.5	10.3	468.1	13.8	509.9	385	34.8	529.8

Table 5: Corresponding evaluations for perforated sections with new web openings

It was observed that when only the angle θ varied, the perforated beams have identical deflections and similar stresses at the 'characteristic' load levels. However, when only the radius R is varied, the bigger it is the higher the deflections and stresses are. It is worth mentioning that as the web openings were plotted in sequence with increasing the area of the inclined web opening, a rational order is found herein. By plotting the results in this way, it was easier to identify the influence of the geometric parameters on the structural performance of the perforated beams. It is worth noting that specimens No.4, No.8 and No.12 experience low stresses and vertical deflections due to the particular combination of θ=40^o and R.

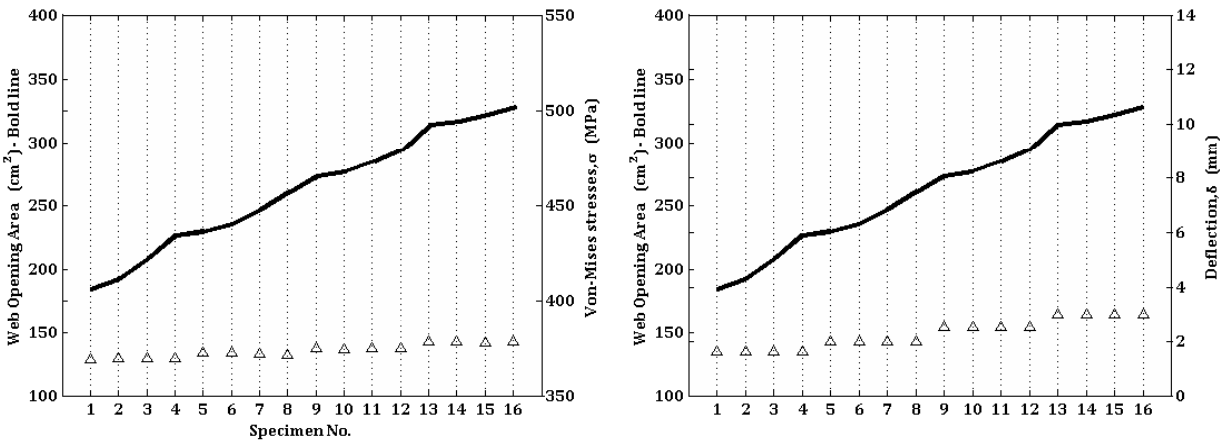

Fig. 12: Von-Mises nodal stresses (left) and maximum vertical deflections (right) at P_y

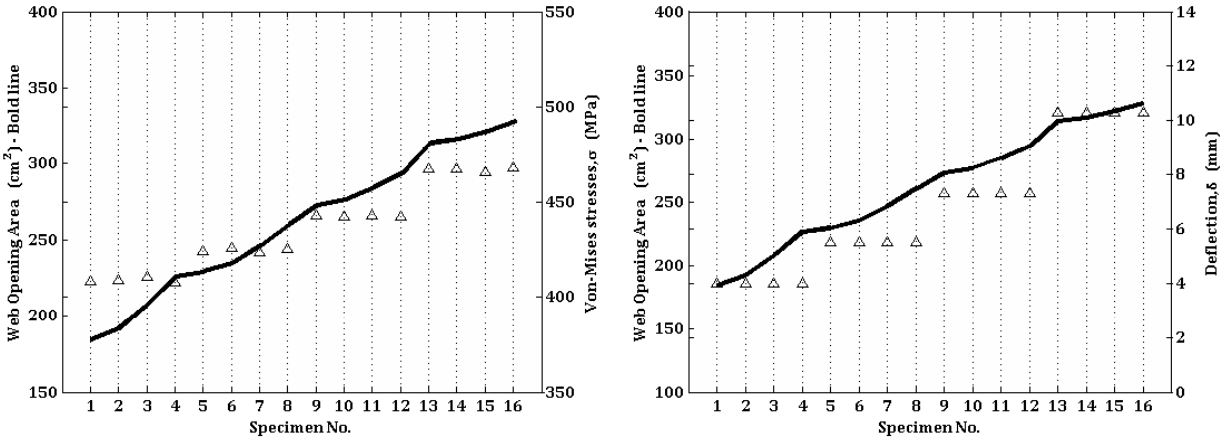

Fig. 13: Von-Mises nodal stresses (left) and maximum vertical deflections (right) at $P_{cr.}$

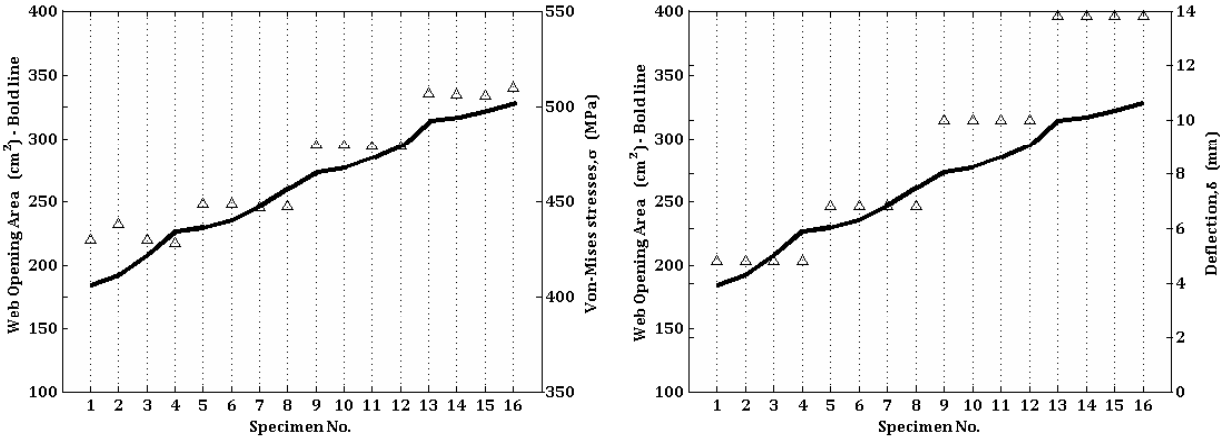

Fig. 14: Von-Mises nodal stresses (left) and maximum vertical deflections (right) at $P_{ult.}$

4.4 Overview of elliptical web openings

It is interesting to examine the stress distribution in the vicinity of the novel web openings at both yield and critical load levels and to visualize the position of the stress concentration points and the formation of the plastic hinges**.** Consequently, the Von-Mises stress distribution of the deformed beams for indicative novel perforated beams are shown in **Fig. 15**, covering the wide range of large vertical and inclined elliptical web opening configuration**.**

Circular (d_o=0.8h) at P_y load level

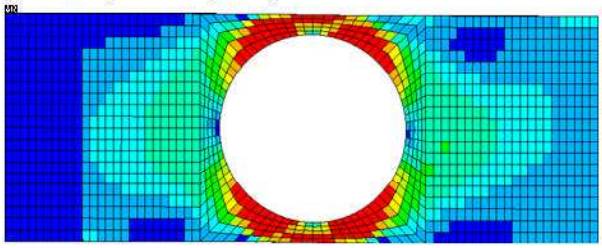

Maximum vertical deflection, δ = 6.0mm
Max. Von-Mises stresses. σ = 398.6MPa

Circular (d_o=0.8h) at P_{ult} load level

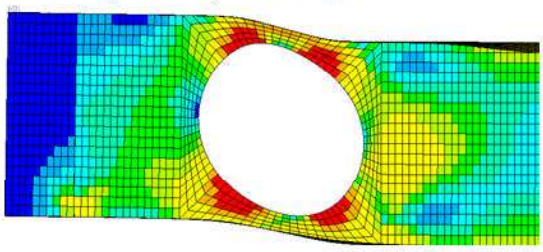

Maximum vertical deflection, δ = 24.7mm
Max. Von-Mises stresses. σ = 526.6MPa

Specimen No.1 Vertical open.

θ10&R0.15 at P_y load level

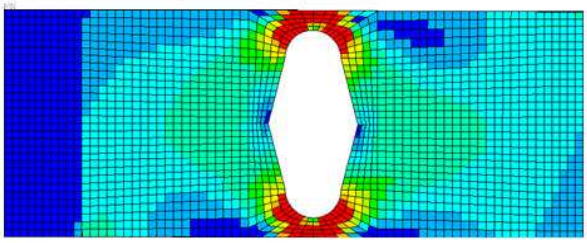

Maximum vertical deflection, δ = 1.4mm
Max. Von-Mises stresses, σ = 369.1MPa

θ10&R0.15 at P_{ult} load level

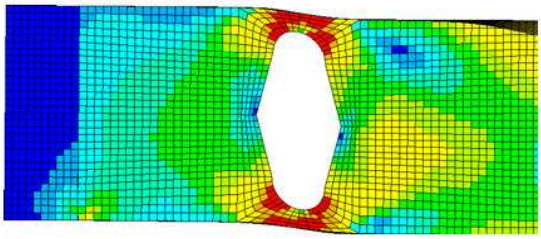

Maximum vertical deflection, δ = 4.7mm
Max. Von-Mises stresses, σ = 429.9MPa

Specimen No.1 Inclined open.

θ10&R0.15 at P_y load level

Left Hand Side

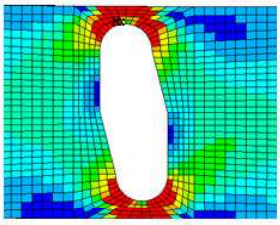

Right Hand Side

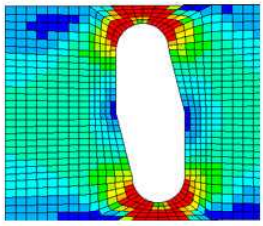

Maximum vertical deflection, δ = 1.6mm
Max. Von-Mises stresses, σ = 369.2MPa

θ10&R0.15 at P_{ult} load level

Left Hand Side

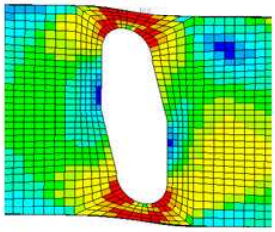

Right Hand Side

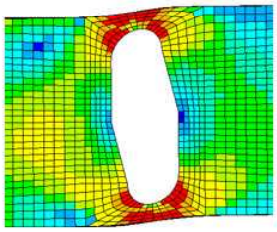

Maximum vertical deflection, δ = 4.8mm
Max. Von-Mises stresses, σ = 4.3MPa

Specimen No.16 Vertical open.

θ40&R0.3 at P_y load level

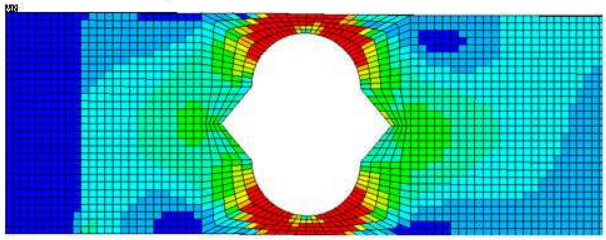

Maximum vertical deflection, δ = 2.8mm
Max. Von-Mises stresses, σ = 376.9MPa

θ40&R0.3 at P_{ult} load level

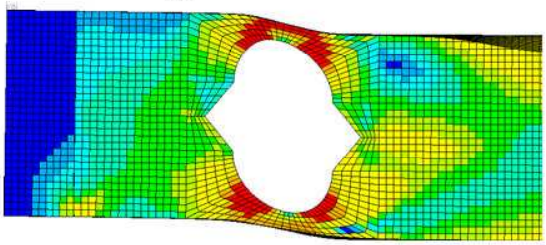

Maximum vertical deflection, δ = 13.7mm
Max. Von-Mises stresses, σ = 500.2MPa

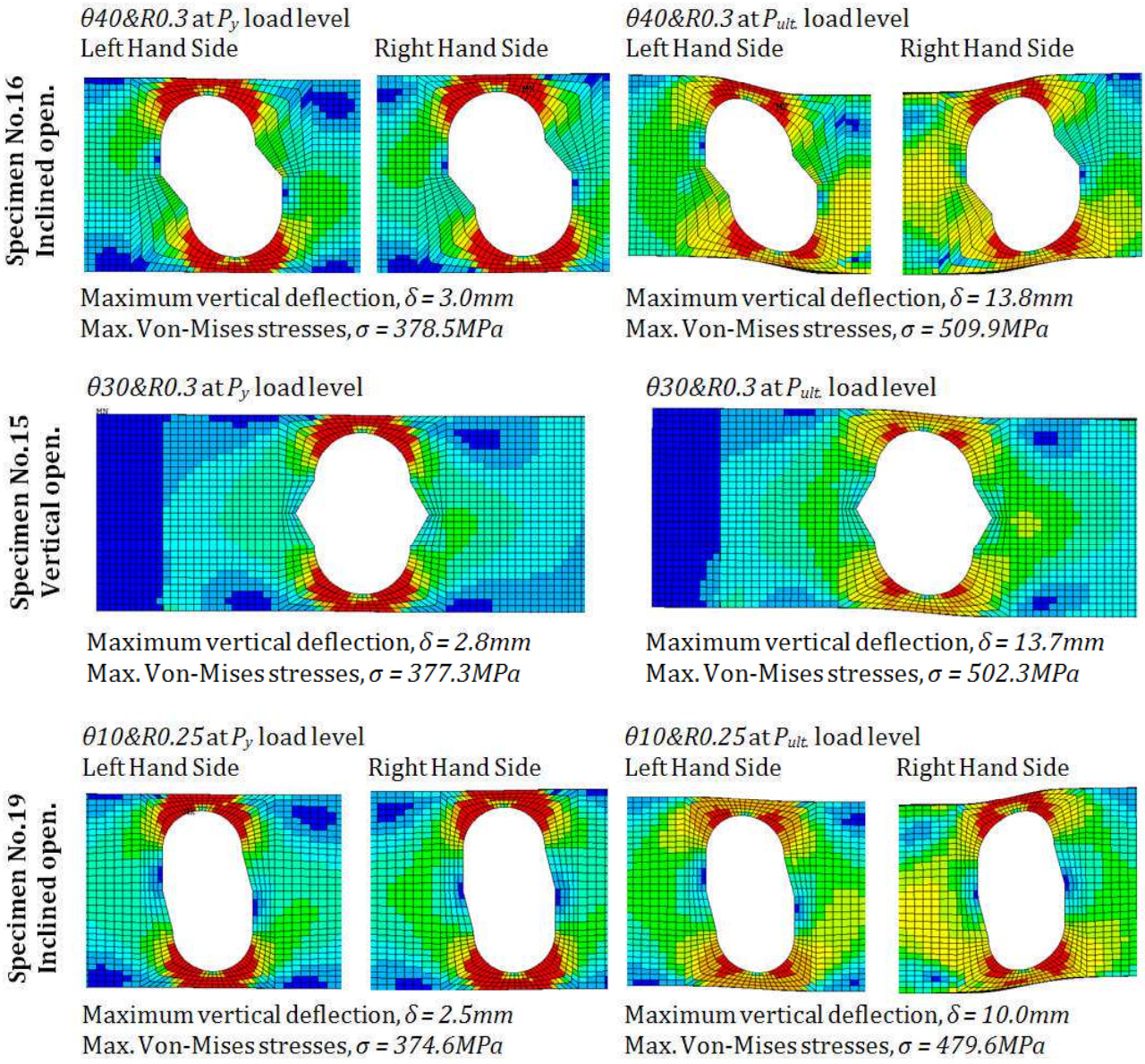

Fig. 15: Maximum vertical deflections and maximum Von-Mises stresses for various novel perforated beams

The maximum deviation of deflections and stresses amongst the perforated beams with circular web openings and their different diameters was found at the 'characteristic' $P_{cr.}$ load level. The maximum deviation in terms of deflections among the perforated beams with any circular and novel elliptical web openings was obtained at the 'characteristic' $P_{ult.}$ load level. Similarly, the maximum deviation in terms of stresses was obtained at the 'characteristic' $P_{cr.}$ load level. In general, higher fluctuation of deflections and stresses amongst the perforated beams with the novel web opening shapes was found as the load level was increased.

All perforated beams with the novel elliptically-based web opening shapes (d_o=0.8h) are stiffer compared to the perforated beams with circular web openings (either d_o=0.8h or d_o=0.76h). Also, smaller

vertical deflections of the novel specimens were always observed. Increased stresses were found at the 'characteristic' load level points P_y and $P_{cr.}$, for the following specimens:

- *Vertical Elliptical Web Openings*
  At P_y: [No.4: *θ30&R0.15*], [No.9, No.11, No.13: *θ20~40&R0.25*] and [No.12, No.14, No.15, No.16: *θ10~40&R0.3*]
- *At* P_{cr}: [No.12, No.14, No.15, No.16: *θ10~40&R0.3*]
- *Inclined Elliptical Web Openings*
  At P_{cr}: [No.13, No.14, No.15, No.16: *θ10~40&R0.3*]

Both vertical and inclined elliptical web openings *θ40&R0.25* (specimens No.13 and No.12, respectively), have relatively large web opening areas, whilst they can be characterised as effective solutions. Furthermore, the vertical elliptical web openings with *θ10&R02.5* (specimen No.7) and *θ40&R0.15* (specimen No.8), and inclined elliptical web openings with *θ40&R0.15* (specimen No.4), indicate the maximum possible difference between the biggest web opening area and deflections and stresses.

From **Table 6** it can be seen that some perforated beams with different combinations of the angle, θ, and radius, R, experience similar stresses at certain 'characteristic' load levels.

Angle, θ, of the straight lines	**Radius of the semi-circles, R**	**Von-Mises Stress estimates, σ**
10^o 20^o	$0.15d_o$	at $P_{ult.}$
10^o 20^o 40^o	$0.2d_o$	at P_y
20^o 30^o 40^o	$0.25d_o$	at P_y
10^o 20^o 30^o 40^o	$0.3d_o$	at P_y

Table 6: Beams with identical results (P-δ curves)

The selection criterion for effective web opening shapes was based on the combination of angle, θ, and radius, R, on the basis that beams are governed by low Von-Mises stresses as well as low vertical deflections. In addition, the combination of θ and R for an effective web opening shape should provide the maximum possible web opening area (i.e. minimum possible beam weight).

5. Shear-moment (V/M) curves for various novel web opening shapes and sizes

5.1 Web opening shapes

A FE parametric study for the novel elliptically-based web opening shapes presented in **Fig. 15** and those presented in another paper [4] studying their web-post buckling strength, was conducted. Three

sizes of web openings (d_o equal to *0.8h*, *0.65h* and *0.5h*) and a mid-range universal beam section commonly used in practice, were used. The aim was to establish the fundamental deviation of the *V/M* interaction curves using perforated beams with the novel web opening shapes proposed in this research paper in relation to simple empirical interaction curves. Hence, perforated beams of UB457x152x52 (S275) and span of 5m, for a total of six vertical and inclined novel elliptical web opening shapes were examined extensively, where the web openings were located at ten different positions along the length of the beam. This covered the cases of pure shear to pure moment actions at the vertical centre-line of the web openings. The aim was to develop the full non-dimensionalised *V/M* interaction FEM curves for direct use in engineering practice. This work is based on the methodology presented in another research paper by the authors [5].

5.2 Summary of the FE model

The FE procedure used for this parametric study is similar to the one presented earlier with only difference being the material properties as a more conservative approach was sought. These were taken as follows:

- Nominal material properties were used for steel grade S275.
- A bi-linear elasto-plastic stress-strain curve with a Young's Modulus, E, of 200GPa and a Tangent Modulus, E_T, of 1000MPa was used, together with a bi-linear kinematic hardening rule and the Von-Mises yield criterion.

5.3 Model of study

The FE model using both geometrical and material non-linearity allowed load redistribution across the web opening following the formation of the first plastic hinge. According to other comprehensive FE studies [5, 6, 13, 16] conducted on beams UB457x152x52, UB457x152x82, UB610x229x101 and UB610x229x140, the mid-range beam size UB457x152x52 was selected to represent the work as it produced the most conservative results. Also, UB457x152x52 has a web thickness of 7.6mm which makes the beam susceptible to web buckling and hence makes it easier to buckle locally and form plastic hinges. 180 non-linear FE runs were conducted herein. In addition, by conducting an investigation on perforated sections with beams of different spans (5, 6, 7.5 and 10m), it was observed that simply supported perforated beams with a span of 5m under a uniformly distributed load provide conservative results.

5.4 Shear-moment (V/M) interaction curves

The *V/M* interaction curves for various novel web openings shapes (as presented in **Fig. 15**) and sizes obtained from the finite element investigation are presented in **Fig. 16**, where the vertical axis is the 'coupled' shear capacity ratio (**Eq. (1)**) and the horizontal axis is the 'coupled' moment capacity ratio (**Eq. (4)**). At failure, the global shear force, $V_{o,Sd}$ (**Eq. (2)**) and the global moment, $M_{o,Sd}$, (**Eq. (5)**) at the centre-line of the openings, are non-dimensionalised with respect to the global section capacities of the perforated sections, $V_{o,Rd}$ and $M_{o,Rd}$, **Eq. (3)** and **Eq. (6)**, respectively.

$$\bar{v} = \frac{V_{o,Sd(FEA)}}{V_{o,Rd}} \tag{1}$$

Where:

$$V_{o,Sd} = w\left(\frac{L}{2} - x\right) \tag{2}$$

and

$$V_{o,Rd} = f_v A_{vo} \geq V_{Sd}, \quad A_{vo} = A_v - d_o t_w, \quad f_v = \frac{0.577 f_y}{\gamma_{Mo}}, \quad A_v = ht_w + 2\left(0.75 t_f^2\right) \tag{3}$$

$$\overline{m} = \frac{M_{o,Sd(FEA)}}{M_{o,Rd}} \tag{4}$$

Where:

$$M_{o,Sd} = wx\frac{(L-x)}{2} \tag{5}$$

and

$$M_{o,Rd} = f_y W_{o,pl} \geq M_{Sd},\ W_{o,pl} = W_{pl} - \frac{d_o^2 t_w}{4} \tag{6}$$

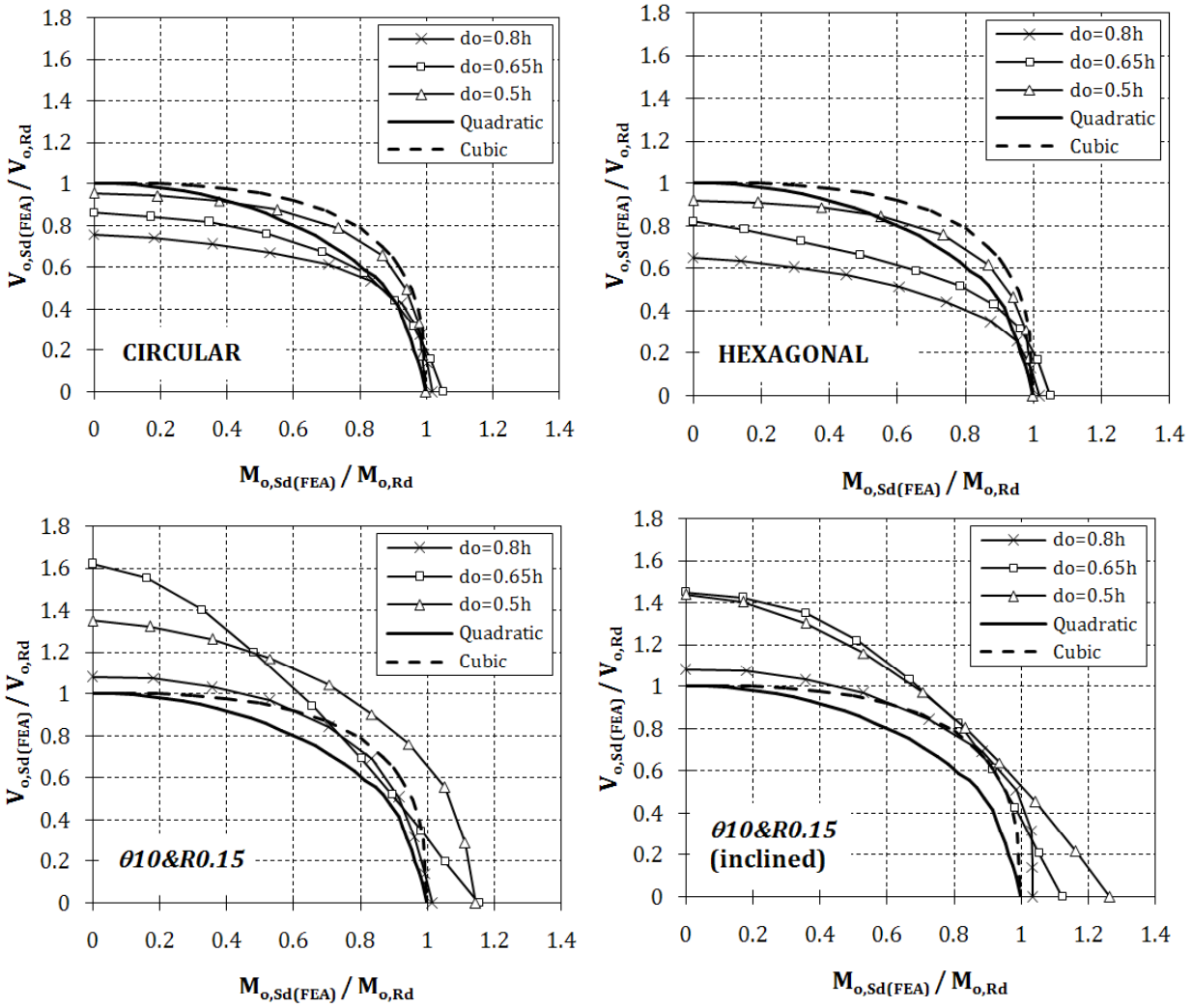

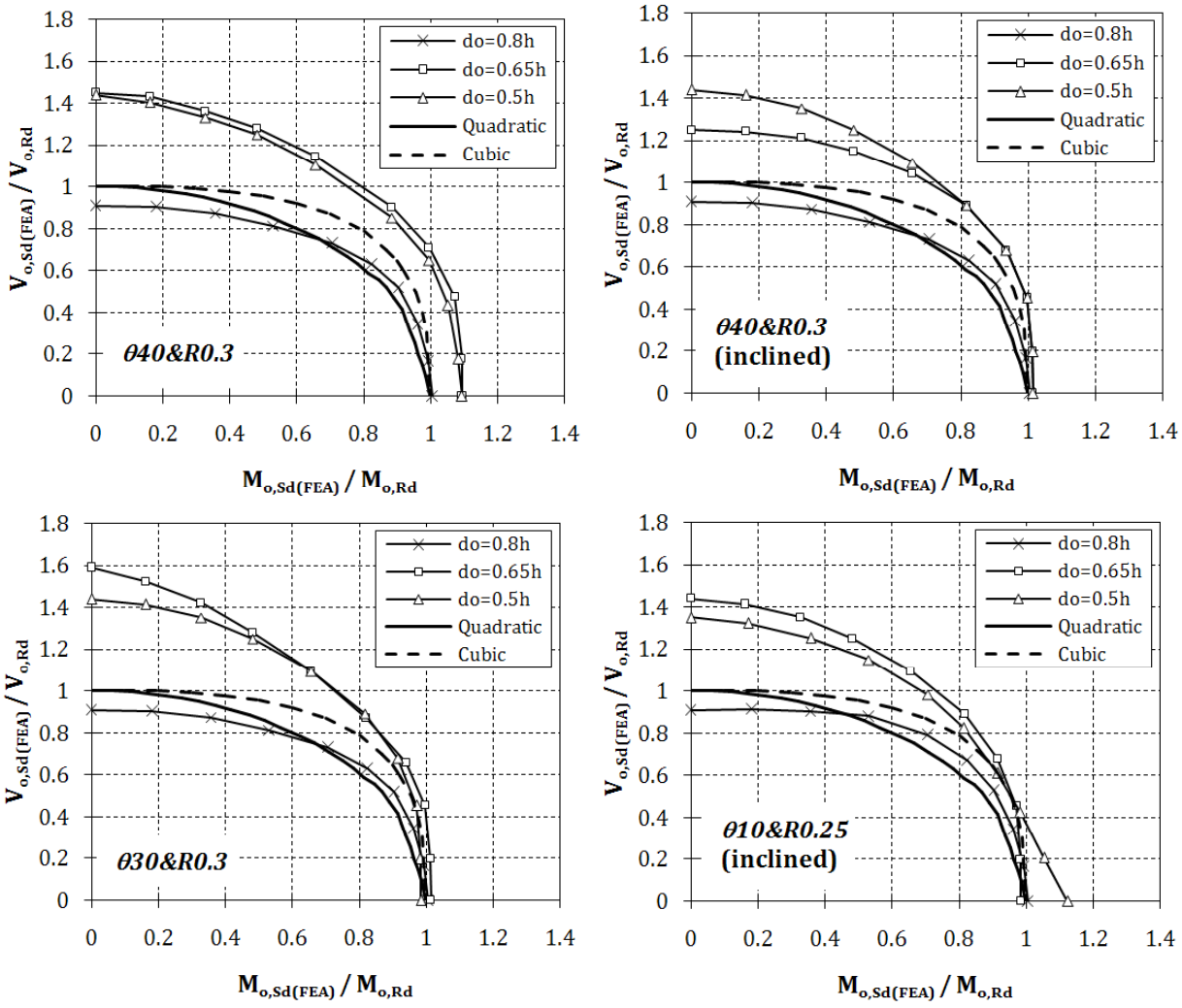

Fig. 16: Non-dimensional *V/M* interaction curves for various novel web opening shapes and sizes

Comparing perforated beams with same size of web openings, d_o, and different values of critical opening length, *c*, the load capacities of the perforated sections should be inversely proportional to the values of *c*. As expected, the increase in the shear capacity is more pronounced when compared to the increase in the moment capacity as the presence of the web opening reduces the shear area of the section significantly, whilst the reduction of the plastic section modulus is small. At times it was seen that the moment ratio is higher than 1.0.

It is also interesting to compare the FEM curves with the simple empirical design quadratic and cubic interaction curves: $\left(\left(V_{Sd}/V_{o,Rd}\right)^2+\left(M_{Sd}/M_{o,Rd}\right)^2=1\right)$ and $\left(\left(V_{Sd}/V_{o,Rd}\right)^3+\left(M_{Sd}/M_{o,Rd}\right)^3=1\right)$ respectively, as they are widely used nowadays for the design of perforated beams. In general, it was observed that both these standard non-linear curves overestimating the capacity of typical perforated beams. Regarding the particular novel web opening shapes, the aforementioned empirical design approaches significantly underestimate the load carrying capacity of the perforated beams. The *V/M* interaction curves of perforated beams with circular and hexagonal web opening shapes are presented for direct comparison in **Fig. 16.**

More analytical, perforated beams with novel web opening shapes present dramatic increase of the shear capacity, especially when the mid- and small-size web openings are used, compared with the traditional perforated beams with circular and hexagonal web openings. A rational overall range of trends of the *V/M* interaction curves compared to the loads estimated in the previous parametric was found. As it was expected, perforated beams with elliptical web openings of diameter, d_o, equal to *0.65h* and *0.5h*, as well as with large radius R, present very close results. It is worth to note that perforated beams with novel vertical elliptical web openings behave slightly better than the ones with novel inclined elliptical web openings. The orientation of the web openings of the perforated beams examined in this particular parametric was chosen so as to represent the worst case scenario (i.e. mirrored to the mid-span), in which the top tee-section is always heavily loaded and the edges of the web openings are stressed.

In more detail, it was observed that perforated beams with d_o equal to *0.8h* and *R* greater than $0.15d_o$ have a 'coupled' shear capacity less than 1.0.

A generalised non-dimensional V/M interaction curve is presented in another paper [5]. This is a non-linear interaction design curve which can be used to allow for an interaction between the shear force and the moment in perforated beams as examined. The design formulas and the methodology evaluating and assessing the Vierendeel capacity of perforated sections using any web opening shapes and sizes is explicitly presented by Tsavdaridis and D'Mello [5]. **Table 7** with *q*, *z* and *k* factors is also presented herein to consider perforated beams with novel elliptically-based web openings. The combination of the factors is not unique, however good agreement between the design curves and the FEM curves is achieved. Otherwise, the 'coupled' shear ratios can be directly picked from **Fig. 16**. **Table 7** (shaded) also summarizes the values of the critical opening length, *c*, and the maximum 'coupled' shear capacity ratios, $\bar{v}$, for perforated sections with web openings subjected under pure shear forces (i.e. position x equal to 1).

Web Opening Depth, d_o		***0.5h***			***0.65h***			***0.8h***			***0.5h***	***0.65h***	***0.8h***
c/d_o	**Factors**	***q***	***z***	***k***	***q***	***z***	***k***	***q***	***z***	***k***	**Maximum $\bar{v}$**		
0.23	**CIRCULAR**	-----	2.5	0.3	-----	1.3	0.3	-----	1.8	0.3	0.95	0.86	0.75
0.423	**HEXAGONAL**	-----	2.0	0.3	-----	1.0	0.3	0.7	1.5	0.4	0.92	0.82	0.65
0.3	***θ10&R0.15* (vertical)**	-----	1.4	0.3	-----	1.0	0.5	-----	2.5	0.5	1.35	1.62	1.08
0.3	***θ10&R0.15* (inclined)**	-----	1.4	0.4	-----	1.5	0.4	-----	2.0	0.3	1.44	1.45	1.08
0.55	***θ40&R0.3* (vertical)**	-----	1.4	0.3	-----	1.5	0.3	-----	2.0	0.3	1.44	1.45	0.91
0.55	***θ40&R0.3* (inclined)**	-----	1.4	0.3	-----	2.0	0.3	-----	2.0	0.3	1.44	1.25	0.91
0.55	***θ30&R0.3* (vertical)**	-----	1.4	0.3	-----	1.5	0.5	-----	2.0	0.3	1.33	1.59	0.91
0.5	***θ10&R0.25* (inclined)**	-----	2.0	0.5	-----	1.5	0.4	-----	2.5	0.3	1.35	1.44	0.91

Table 7: Summary of the factors for all perforated sections and maximum 'coupled' shear capacity ratios

6. Summary

A UB305x165x40 (S355) with two circular web openings (d_o=*0.76h*) was tested experimentally to obtain the failure mode and load carrying capacity. Stresses in the vicinity of the web openings and maximum vertical deflections were acquired, whilst 'characteristic' yield, critical and ultimate load level points were recorded and used as a reference in the optimisation study of the novel web opening shapes. A comprehensive FE investigation on perforated beams with circular and novel web opening shapes was carried out, after the typical FE model was validated against the experimental results. The beam model examined was a mid-range deep thin-webbed steel beam with isolated large web openings, subjected to high shear forces.

The widely-used method of using *V/M* interaction curves has been enhanced by using the FEM. Results of analyses of a mid-range perforated section with various novel elliptically-based web opening configurations presented for first time, show how the Vierendeel mechanism is affected not only by the size, but also by the shape of the web openings. In total, the effects of the flange and web thicknesses, the critical opening length and depth as well as the web opening shape were incorporated in the parametric FE investigation. The investigation on novel web openings presented positive results that advance current knowledge. Finally, the global 'coupled' shear capacities of four mid-range perforated sections with six particular effective web opening shapes, covering a wide range of novel configurations, can be either obtained directly from the *V/M* interaction FEM curves developed or using the design formulas and the methodology presented by the authors [5] together with the factors given in **Table 7.**

Further concluding remarks can be drawn as follows:

- It was found that perforated beams with circular web openings with diameter, d_o, equal to *0.76h* and *0.8h* have considerably different stiffness following the yielding point.
- All perforated beams with novel elliptical web openings (d_o=*0.8h*), present increased stiffness, mainly in the plastic region. It was remarkable that their maximum vertical deflections at the 'characteristic' load levels are lower than perforated beams with circular web openings with a smaller diameter (d_o=*0.76h*).
- The stresses in the vicinity of the web openings were affected by both θ and R geometrical parameters of the novel web opening shapes. However, the deflections of the perforated beams are only affected by radius, R, as it is the main parameter which determines the web opening area and the critical opening length, c, at the top and bottom tee-sections.
- Changing parameter, θ, led to significant variation of the Von-Mises stresses in the vicinity of the vertical elliptical web openings, whereas slight variation takes place in the vicinity of the inclined elliptical web openings. It should be mentioned that the angle θ changes the strength of the web-post dramatically by changing its effective width, in case that web openings are closely spaced.

The largest ever web openings of dimensions equal to 80% of the depth of beams were used in this research programme in order to produce light-weight beams as well as deeper sections when they manufactured by using the proposed profile cutting procedure [3]. With regard the large cut-outs, a more conservative design approach can be achieved now, applying the results of the current study (with all web opening diameters, d_o equal to *0.8h*) on traditional perforated beams with web openings with d_o equal to *0.75h*. A new structural form of perforated beams was proposed and examined for first time offering a new architectural perspective within an environmentally friendly approach, in terms of steel fabrication and construction. A reduced production time and substantial material saving which meet the economic requirements, ensuring safety and structural performance makes such novel steel perforated beams worth considering [6].

References

[1]http://www.asdwestok.co.uk/ (visited in 05/03/12)

[2]Sweedan AMI, El-Sawy KM. Elastic local buckling of perforated webs of steel cellular beam-column elements. Journal of Constructional Steel Research, 2011, Vol. 67 (7):1115-1127, doi:10.1016/j.jcsr,2011.02004.

[3] Tsavdaridis, KD, D'Mello C. (Inventors), City University, London (Proprietors). Filed Patent (No GB1112512.7): Perforated Structural Beams. Intellectual Property Office, 2011.

[4]Tsavdaridis KD, D'Mello C. Web Buckling Study of the Behaviour and Strength of Perforated Steel Beams with Different Novel Web Opening Shapes. Journal of Constructional Steel Research, 2011; 67(10):1605-1620, DOI: 10.1016/j.jcsr.2011.04.004.
[5]Tsavdaridis KD, D'Mello C. Vierendeel Bending Study of Perforated Steel Beams with Various Novel Web Opening Shapes, through Non-linear Finite Element Analyses. Journal of Structural Engineering-ASCE, 2011, ISSN (print): 0733-9445 & ISSN (online): 1943-541XDOI:10.1061/(ASCE)ST.1943 541X.0000562.
[6]Tsavdaridis KD. Performance of perforated steel beams with novel web openings and with partially concrete encasement. PhD Thesis, City University, London, March 2010.
[7]Tsavdaridis KD, D'Mello C. Finite element investigation of perforated steel beams with different web opening configurations. 6th International Conference on Advances in Steel Structures (Hong Kong China December 16-18, 2009) ICASS'09/IJSSD/IStructE Asia-Pacific Forum, Hong Kong, China, 2009; 213-220.
[8]Redwood RG. Design of beams with web holes. Canadian Steel Industry Construction Council, Willowdale, Ontario, Canada, 1973.
[9]Redwood RG. The strength of steel beams with unreinforced web holes. Civil Engineering and Public Works Review, 1969.
[10]Redwood RG, McCutcheon JO. Investigation on Vierendeel mechanism in steel beams with circular web openings. Journal of Structural Division, 1968, Proc ASCE; 94(ST1):1-17.
[11]Bower JE. Design of beams with web openings. Journal of the Structural Division, 1968, Proc ASCE; 5869(ST3):783-807.
[12]Ward JK. Design of composite and non-composite cellular beams. The Steel Construction Institute, SCI Publication 100, 1990.
[13]Chung KF, Liu TCH, Ko ACH. Steel beams with large web openings of various shapes and sizes: an empirical design method using a generalized moment-shear interaction. Journal of Constructional Steel Research, 2003; 59:1177-1200.
[14]Tsavdaridis K.D, D'Mello C, Hawes M. Experimental study of ultra shallow floor beams with perforated steel sections. 11th Nordic Steel Construction Conference (Malmö Sweden September 2-4, 2009) NSCC2009 Press, Malmö, Sweden, 2009; 312-319.
[15]BS EN 10002-1:2001. Tensile testing of metallic materials; Method of test at ambient temperature. BSI, 2001.
[16]Chung KF, Liu TCH, Ko ACH. (2000) Investigation on Vierendeel mechanism in steel beams with circular web openings. Journal of Constructional Steel Research, 2000; 57:467-490.

Notations

A_v	Shear area of the un-perforated section
A_{vo}	Reduced shear area of the perforated section
c	Critical opening length
d_o	Diameter (Depth) of the web opening
f_y	Design yield strength of the steel
f_v	*S*hear strength of the steel
h	Overall depth of the steel beam
L	Span of the specimen
m	Moment utilisation ratio ($m=M_{Sd}/M_{o,Rd}$)
$\overline{m}$	'Coupled' moment capacity ratio
$M_{o,Rd}$	Moment capacity of the perforated section
$M_{o,Sd(FEA)}$	Global 'coupled' moment capacity of perforated sections as obtained from FEA
M_{Sd}	Applied global bending moment at centre-line of the web opening

P_y	'Characteristic' yield load
$P_{cr.}$	'Characteristic' critical load
$P_{ult.}$	'Characteristic' ultimate load
R	Radius of the of the semi-circles at the top and bottom tee-sections at the novel non-standard elliptical web openings
θ	Angle of the strain lines at the novel non-standard elliptical web openings
v	Shear utilisation ratio ($v=V_{Sd}/V_{o,Rd}$)
$\bar{v}$	'Coupled' shear capacity ratio
$V_{o,Rd}$	Shear capacity of the perforated section
$V_{o,Sd(FEA)}$	Global 'coupled' shear capacity of perforated sections as obtained from FEA
V_{Sd}	Applied global shear force at centre-line of web opening
w	Failure uniformly distributed load as obtained from FEA
W_{pl}	Plastic modulus of the overall section
γ_{Mo}	Partial safety factor (taken as unity for conservative design purposes)